Applied Thermal Engineering 71 (2014) 581–588

Contents lists available at ScienceDirect

Applied Thermal Engineering

journal homepage: www.elsevier.com/locate/apthermeng

Experimental investigation of pump-assisted capillary phase change loop

C. Jiang, W. Liu*, H.C. Wang, D.D. Wang, J.G. Yang, J.Y. Li, Z.C. Liu*

School of Energy and Power Engineering, Huazhong University of Science and Technology, Wuhan 430074, PR China

HIGHLIGHTS

- A pump-assisted capillary phase change loop is presented.
- Both mechanical pump and capillary force are used for driving the working fluid.
- Test results show that no obvious temperature oscillation is observed.
- The loop can operate 17.7 W/cm^2 × 1850 mm at the heater surface temperature below 80 °C.
- Initial distribution of working fluid has impact on the operation characteristics.

ARTICLE INFO

Article history:
Received 14 May 2014
Accepted 28 June 2014
Available online 19 July 2014

Keywords:
Pump-assisted
Phase change
Heat transfer
Oscillation
Different working conditions

ABSTRACT

This paper presents an overview of a novel two-phase loop called "pump-assisted capillary phase change loop" designed to address the drawbacks of temperature oscillation and limited heat transfer distance in loop heat pipes. The proposed loop is a combination of active and passive systems. It is equipped with an evaporator designed in the type of flat-disk, and a biporous wick that provides the capillary force. In addition, methanol is chosen as the working fluid. During the heat-transfer process, the working fluid is transferred by both the capillary force and the driving force of the mechanical pumping. Both the sensitive and the latent heat of the working fluid are utilized to transfer heat. The liquid circulation through the compensation chamber takes away heat leak from the evaporator to the compensation chamber. Test results indicate that the system shows a very fast response to variable heat loads with no obvious temperature oscillation being detected. The maximum heat load the system could transfer increases up to 180 W (heat flux = 17.7 W/cm^2) with transport distance of 1850 mm at the heater surface temperature below 80 °C, when the power input of the mechanical pump is 2 W. The evaporator thermal resistance varies between 0.298 K/W and 0.196 K/W at the heat sink temperature of −10 °C.

1. Introduction

At present, cooling technologies are widely used in aerospace, energy, and other fields. Cooling technology could be divided into two broad categories—active and passive—based on the power source of the system. Active cooling systems, such as micro-channel and micro-jet loops, rely on a mechanical pump to drive the working fluid, while passive systems like loop heat pipe (LHP) and capillary pumped loop (CPL) use capillary force to transport heat. Both approaches have their advantages and disadvantages. Active systems are characterized by controllability and long transport distance. However, restricted to single-phase heat transfer, in order to dissipate high heat fluxes, they would suffer from a drastic pressure drop, resulting in extremely high power input of the mechanical pump. On the other hand, LHP is an efficient two-phase heat transfer device [1]. The capillary pump facilitates circulation of the working fluid [2]. The maximum heat load and transport distance of LHP are highly dependent on the capillary force. For a flat miniature LHP, the maximum heat load and transport distance sharply decrease [3–11]. For the LHP system with methanol as the working fluid, Liu et al. [10] have tested an LHP with the transport distance of 300 mm. The heat load reaches 160 W (heat flux 16.8 W/cm^2) when the evaporator wall temperature is below 85 °C. Li et al. [11] have developed an LHP with flat disc-shaped evaporator. The system reaches 100 W (heat flux 10.4 W/cm^2) at the evaporator wall temperature below 75 °C and the heat transport distance is 360 mm. Temperature oscillation, which is also observed in LHP, has a significant impact on the performance of the system.

* Corresponding authors.
E-mail addresses: w_liu@hust.edu.cn (W. Liu), zcliu@hust.edu.cn, zcliuqd@gmail.com (Z.C. Liu).

http://dx.doi.org/10.1016/j.applthermaleng.2014.06.065
1359-4311/

Nomenclature

P	pressure, Pa
Q	heat load, W
W	pumping power, W
T	temperature, °C

Subscripts

V	vapor
l	liquid
sink	heat sink
pump	mechanical pump

Abbreviations

Evap-out	evaporator outlet, T6
Wall	heater surface, T1~T4
CC-in	compensation chamber inlet, T19
CC-out	compensation chamber outlet, T17
CC-wall	compensation chamber wall, T5
Cond-#1 inlet	condenser #1 inlet, T10
Cond-#2 inlet	condenser #2 inlet, T11
Amb	ambient

Temperature oscillation in LHP is mainly caused by the liquid–vapor interface fluctuation inside the system [12–18]. J. Ku et al. [12,15] showed that loop operating temperature was dependent on the compensation chamber temperature. Both the returning sub-cooled liquid and the heat leak from the evaporator oscillating would cause the compensation chamber temperature to oscillate, leading to temperature oscillations in the rest of the loop. Mo [13] analyzed the test results and inferred that the position of the vapor–liquid interface inside the condenser varied with the temperature oscillations, resulting in liquid–vapor interface motion in the compensation chamber. Y. Chen et al. [14] studied a miniature LHP under varying heat sink temperatures, heat loads, and orientations. They deduced that the change of liquid–vapor distribution between compensation chamber, evaporator, and condenser caused the temperature oscillations. R. Singh et al. [16] proposed that the oscillation occurring in LHP was dependent on the thermal and hydrodynamic conditions inside the compensation chamber. Zhang et al. [17] found that the temperature oscillation in LHP occurred partly because of the restructuring of the phase distribution of the working fluid in the compensation chamber owing to heat leak from the evaporator to the compensation chamber. Gai [18] supposed that the vapor bubble condition inside the compensation chamber was mainly determined by the heat leak from the evaporator to the compensation chamber, the heat loss to the ambient, and the temperature and rate of sub-cooled liquid. The growth rate of the vapor bubble or dissipation inside the compensation chamber determined the nature of temperature oscillation.

In order to solve the problems of temperature oscillation and limited heat transport distance in LHP, a novel two-phase device called “pump-assisted capillary phase change loop” has been designed. The loop consists of an evaporator, a mechanical pump, a reservoir, an ejector, and a condenser. A schematic of the system is showed in Fig. 1. The loop is a combination of active and passive systems. Working fluid is transferred by both capillary force and mechanical pumping. The evaporator is the core component for absorbing waste heat of the electronic device. Both sensitive heat and latent heat of the working fluid are utilized to transfer heat. During the heat-transfer process, the mechanical pump forces liquid to circulate in the loop, thereby providing liquid for wick boiling and taking away heat leak from the evaporator to the compensation chamber. Hence, the vapor phase in the compensation chamber is restrained owing to the forced liquid circulation. The mechanical pumping in the loop significantly increases the liquid transport distance and improves the robustness of the system, while the porous wick prevents the liquid and vapor from penetrating. The separation of liquid and vapor flow into different lines helps prevent a large pressure drop, thus decreasing the pumping power.

In recent years, many researchers have experimentally studied the operating principles of pump-assisted capillary phase change loop [19–25]. It has been investigated for its potential to the thermal control of electronic devices [21]. These different types of systems show that pump-assisted capillary loop has many advantages, such as high heat flux dissipation and long transport distance [20]. Experimental results have shown that some parameters, including system pressure, liquid velocity, heat load, and heat sink temperature, have a significant impact on the operating temperature of the device [24,25]. There are some differences between the previous works and the loop proposed in this work. In the two-phase loop concept [19,21], the mechanical pump forces liquid

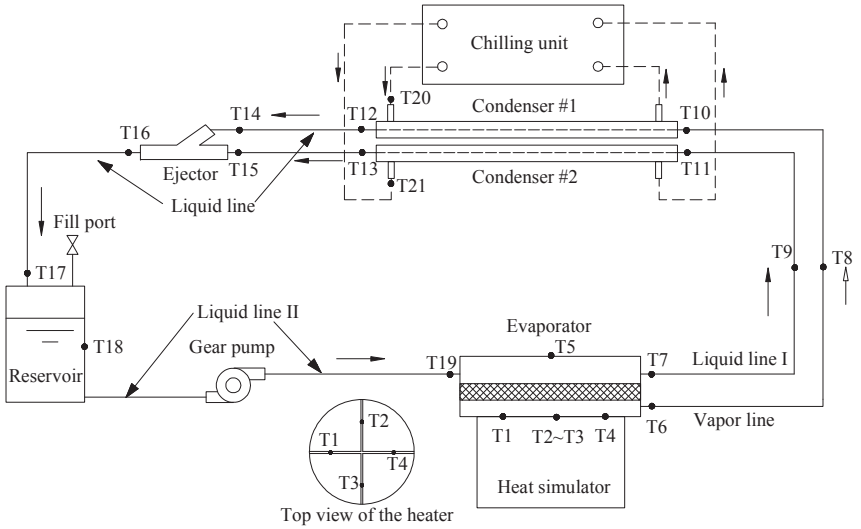

Fig. 1. Schematic of the pump-assisted capillary phase change loop and locations of the main thermocouples.

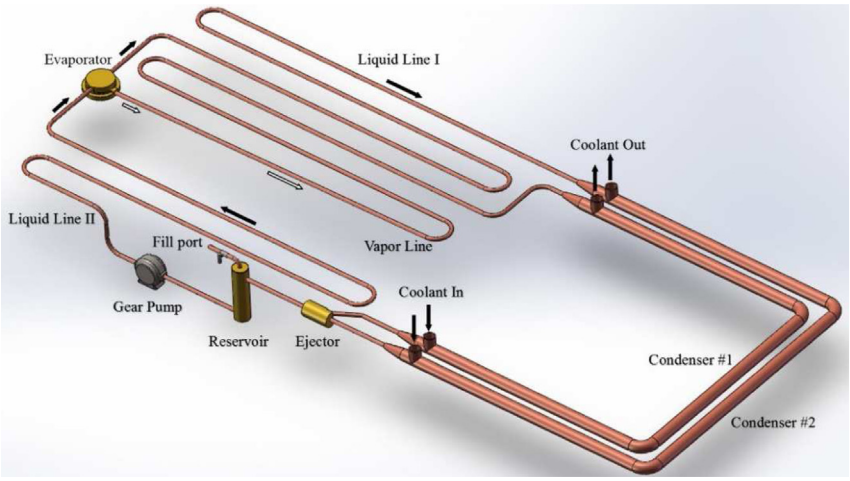

Fig. 2. A 3-D model of the experimental system.

directly into the evaporator and no bypass line is added on the compensation chamber. Thus, a great pressure drop is detected and the porous wick is always flooded. T. Hoang et al. [22,23] adopt a cylinder evaporator in the system which is complicated to contact with the surface to be cooled. The reservoir placed in their loop is designed for the thermal control of the loop. The components of the loop presented by C. Park [24,25] are different from this work. The reservoir in their loop is used to condense the vapor and to contain the excess liquid simultaneously.

In this study, a pump-assisted capillary phase change loop is set up and a flat-disk-shaped evaporator is designed. The objective of this investigation is to determine the operational characteristics of the system during start-up and steady state operation, and to provide a thorough understanding of the pump-assisted capillary phase change loop.

2. Experimental setup

A 3-D model of the experimental system is presented in Fig. 2. The evaporator is designed in the type of flat-disk with the diameter (d_1) of 45 mm and thickness (h) of 16.5 mm. Such an evaporator easily remains in contact with the surface to be cooled. The evaporator is made of brass with the wall thickness of 1.5 mm. A cross section of the evaporator is shown in Fig. 3. A series of rectangular channels are set up as vapor channels on the inside of the evaporator active heat zone. The top of the channels are assembled tightly with porous wick. Consequently, the vapor chamber is formed between the interface of the wick and the internal wall of the heat zone. The biporous wick is made of sintered nickel. The structure of the wick has been reported in our previous works [10,11,26]. The compensation chamber, which supplies liquid for wick boiling, is formed between the wick and the evaporator wall. A liquid inlet and outlet are designed on the side wall of the compensation chamber. As the liquid gets through the compensation chamber, the heat leak from evaporator to the compensation chamber is taken away.

Double-pipe heat exchanger is selected as the condenser for the set up. There are two sets of condensers in the system, use independently to condense the vapor from the vapor chamber and to cool the liquid from the compensation chamber. Meanwhile, the two condensers can be integrated together to form a compact system. The ejector is applied to join the liquid together. The reservoir contains the extra liquid that insures operation safety of the mechanical pump. A charging line is fixed on the reservoir for vacuumizing the loop and charging the working fluid. A magnetic drive gear pump is selected for driving the working fluid in the system. The nominal flow range of the pump varies between 20 ml/min and 1000 ml/min. The nominal pressure is 7 bar [27]. The transport line is made of pure copper with an inner diameter of 3.5 mm. In order to accomplish a decrease in the heat exchange with the ambient, all the components are insulated with a thermal insulation material. Methanol is chosen as the working fluid and the liquid charge ratio is 75%. Detailed structural parameters of the system are as shown in Table 1. To avoid the impact of non-condensable gas on the operational characteristics, the loop is evacuated. The predetermined working fluid is filled into the loop only once all possibility of a leak is eliminated.

For the purpose of testing the thermal performance of the loop under variable heat loads, a heat simulator with an active diameter of 36 mm is made of a copper block with three embedded cartridge heaters. A 10 mm thick nano-adiabatic material is used to insulate the heat simulator and the heat loss to ambient is evaluated to be less than 0.5% of the heat load. A wattmeter with a relative error of 0.5% is used for measuring the input heat power. Twenty-seven

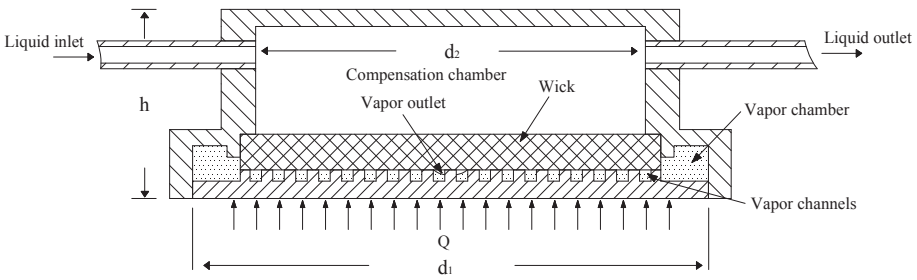

Fig. 3. Cross section of the evaporator.

Table 1
The main parameters of the system.

Parameter	Material	Value	Unit
Evaporator	Brass		
Diameter, d_1		45	mm
Thickness, h		16.5	mm
Compensation chamber diameter, d_2		34	mm
Porous wick	Nickel		
Diameter		36.7	mm
Thickness		3.1	mm
Porosity		70	%
Porous radius		2.6–53	μm
Permeability		7.6×10^{-13}–7.9×10^{-13}	m^2
Vapor line	Pure copper		
Length		1850	mm
Inner diameter		3.5	mm
Liquid line	Pure copper		
Length I		1880	mm
Length II		1580	mm
Inner diameter		3.5	mm
Condenser #1	Pure copper		
Length		1240	mm
Condenser #2	Pure copper		
Length		1480	mm
Reservoir	Brass		
Height		80	mm
Diameter		20	mm
Ejector	Brass		
Volume		0.34	ml

thermocouples with ±0.2 °C accuracy measure the temperature at different locations of the loop. Fig. 1 shows the placement of the main test points. The heater surface temperature is presented by the temperature measured at the cross groove of the heater wall as shown in Fig. 1. The average temperature of T1~T4 is adopted as the heater surface temperature. All the thermocouples are connected to "Keithley 2700" data acquisition system that helps record the temperature variations of the loop at an interval time of every 4 s. The input power of the mechanical pump is measured by a digital power meter with an accuracy of 0.2%. The loop is tested at the horizontal position with the evaporator and the condenser at the same level. The ambient temperature is around 28 °C throughout the test periods.

3. Results and discussions

3.1. Start-up tests

The start-up procedure involves startup of the mechanical pump and the heat load. It is crucial to evaluate the design and reliability of the loop during the start-up tests. Before the heat load is applied, liquid in the reservoir must be forced by the pump to circulate in the loop. This allows enough liquid to be accumulated by the porous wick for evaporation. Fig. 4 shows the start-up process under different heat loads at a heat sink temperature of −10 °C. The system could thus achieve a steady state under different operating conditions with the temperature profiles showing similar trends except for the notable difference in the condenser #1 inlet temperature. From the test results, two different conditions of working fluid in the evaporator are revealed through the temperature difference between the evaporator outlet and condenser #1 inlet.

During the operation, mechanical pump forces liquid into the compensation chamber. Liquid pressure in the compensation chamber is P_l. As the heat load is applied, heat flux spreads to the porous wick, causing liquid evaporation on the surface of the wick. Consequently, vapor is formed in the vapor chamber with a pressure of P_v. Under low heat loads, as seen in Fig. 4(a), a poor vapor pressure is generated with $P_v < P_l$. As a result, liquid is driven into

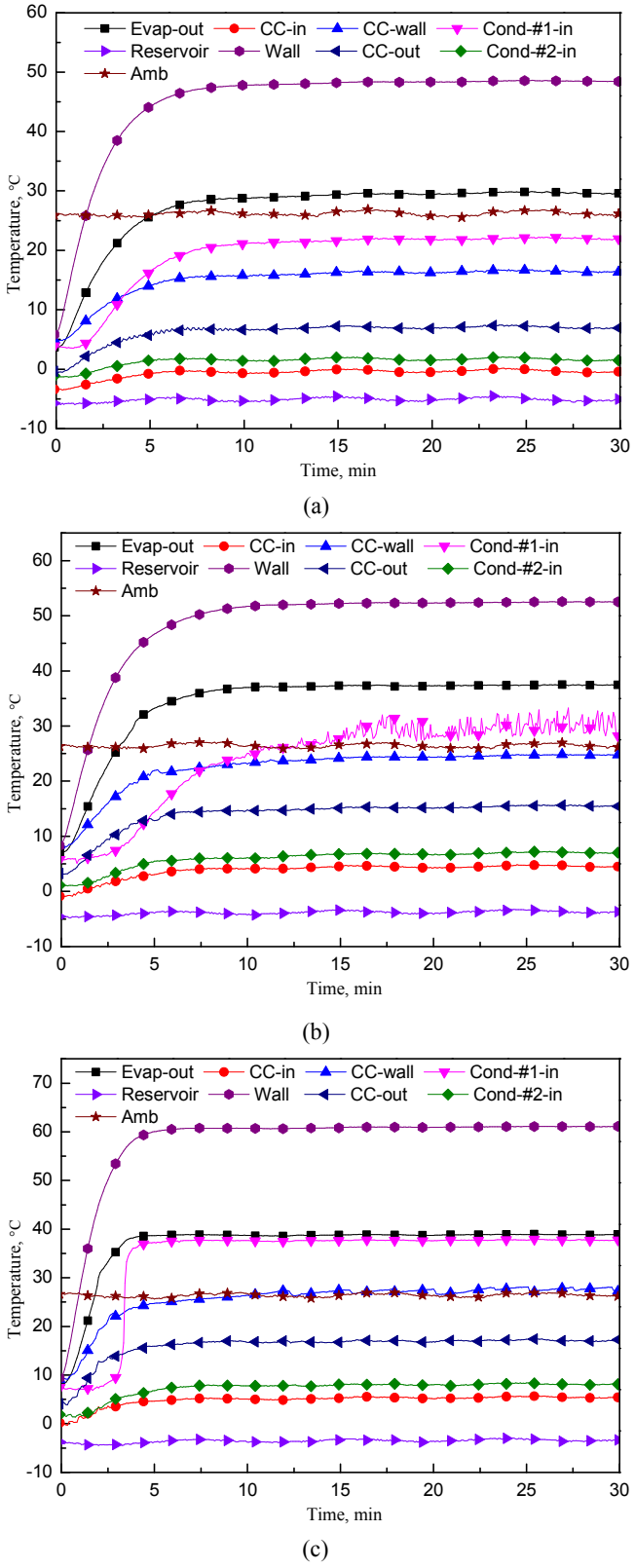

Fig. 4. Start-up of the system at different working conditions. (a) W_{pump} = 2 W, Q = 80 W, T_{sink} = −10 °C. (b) W_{pump} = 1.6 W, Q = 70 W, T_{sink} = −10 °C. (c) W_{pump} = 1.6 W, Q = 110 W, T_{sink} = −10 °C.

the vapor chamber due to the pressure difference thereby flooding the wick [15]. At the condenser #1 inlet, liquid is rapidly cooled due to the back heat conduction of the condenser [28]. Therefore, a great temperature difference of the evaporator outlet and the condenser #1 inlet is observed as seen in Fig. 4(a). With an increase of the heat load, a proper boiling is gradually set up in the porous wick with no occurrence of wick flooding and the vapor occupies the entire vapor chamber. As illustrated in Fig. 4(c), a remarkable jump of condenser #1 inlet temperature is observed as soon as the vapor transfers to the condenser #1. When the steady state condition is achieved, the temperature difference between the evaporator outlet and the condenser #1 inlet is negligible.

Fig. 4(b) shows a slow generation of vapor in the vapor chamber corresponding to comparatively low heat flux, while the vapor–liquid interface inside condenser #1 moves back and forth around the condenser #1 inlet. Consequently, a temperature oscillation occurs at the condenser #1 inlet. In comparison with the three different heat processes, start-up time required for low heat loads is greater than that of high heat loads.

3.2. Variable heat load tests

Variable heat load tests of the system help in evaluating the reliability and transient response to different working conditions. In these tests, heat load is varied in fixed steps while the pumping power increases at an interval of 0.2 W. The heat load is increased or decreased in increments of 10 W. At the maximum heat load, the heater surface temperature is below 80 °C. During the operations, heat sink temperature is around 10 °C. It can be observed that, for all the tests, the system presents very fast response to the input heat power and similar trends of temperature profiles are noticed under three different pumping powers. Similar to the start-up processes presented earlier, the temperature difference between the evaporator outlet and the condenser #1 inlet distinguish the two different kinds of working conditions in the evaporator. For the input heat power less than 50 W, 60 W, and 70 W as seen in Fig. 5(a)–(c) respectively, single-phase heat transfer is the primary method for dissipating the input heat power. Therefore, the increment of the heater surface temperature for each step of heat load increment is relatively large. For high heat loads, beyond 50 W, 60 W, and 70 W as seen in Fig. 5(a)–(c) respectively, the menisci in the wick set up and the wick is no longer flooded. Proper boiling takes place in the evaporator with the phase change process playing a dominant role. If the heat loss to the ambient is neglected occurring during the transmission, the evaporator outlet and condenser #1 inlet are recorded with the same value of around 42.5 °C. Under such circumstances, each step of heat load increment leads to a smaller increase of the heater surface temperature.

Fig. 5 shows that an increase of the pumping power causes the wick boiling in the evaporator to correspond accordingly to the increasing heat flux. This may be caused by two factors as follows: (1) With an increase of the pumping power, mass flow rate of liquid through the compensation chamber increases, leading to the enhancement of heat convection in the compensation chamber. Eventually, heat leak from evaporator to the compensation chamber grows larger. (2) Liquid pressure in the compensation chamber increases due to an increase of the pumping power. In order to maintain a proper boiling in the wick, vapor pressure in the vapor chamber should be larger than the liquid pressure, thereby resulting in a greater vapor mass requirement. These two factors point to a higher heat flux being noted.

The initial distribution of working fluid in the evaporator has a great influence on the operational characteristics. With the increase process at 100 W, as seen in Fig. 5(a), where phase change process has taken place in the evaporator, the heater surface temperature rises in the first stage, and subsequently decreases. This heat input eventually results in a steady state. Thereafter, the same heat load of 100 W obtained during the decline process, results in a variation of the heat surface temperature profile. Similar trends are observed in other two pumping powers. This variation of temperature profile is discussed in the following section.

3.3. Impact of the initial distribution of working fluid

In variable heat load tests, the interval time between the different pumping power tests is longer than 12 h. During the

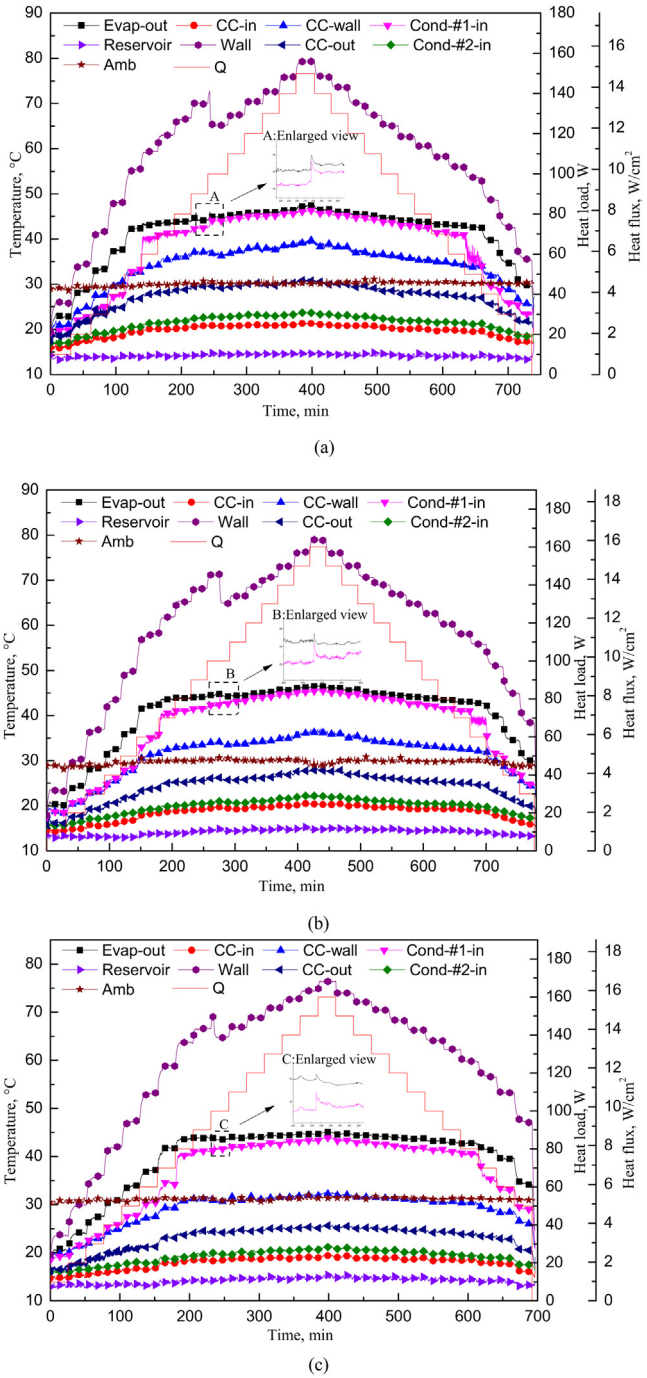

Fig. 5. Performance tests of the system for heat load changing in regular steps at different pumping powers. (a) W_{pump} = 1.6 W, T_{sink} = 10 °C. (b) W_{pump} = 1.8 W, T_{sink} = 10 °C. (c) W_{pump} = 2.0 W, T_{sink} = 10 °C.

periods of no heat input, vapor in the evaporator is condensed completely and the generated liquid partially occupies the vapor channels with the help of gravity. As the heat flux turns on and increases gradually, the menisci set up in the wick. Capillary force drives liquid for evaporation and replenishes the decrease of liquid in the vapor channels owing to the phase change process. When the heat flux reaches high enough, e.g. 100 W in Fig. 5(a), the requirement of liquid for evaporation increases. Finally, no additional liquid is fed to the vapor channels and the earlier accumulated liquid vaporizes after superheating. This enhances the capability of heat transfer in the evaporator. Consequently, a prominent drop of heater surface temperature is observed. At the same time, owing to a larger vapor generation, vapor flow rate increases at the evaporator outlet. Afterward, heat exchange between vapor and the ambient decreases. As showed in the enlarged view of "A zone" in Fig. 5(a), a spike of the evaporator outlet and the condenser #1 inlet temperature appears.

In order to validate the influence of initial distribution of working fluid in the evaporator, a special test is carried out. As seen in Fig. 6(a) and (b), the heat sink temperature and the pumping power keep the same value of −10 °C and 1.6 W, respectively. The only difference is that, before the increase process of the heat load in Fig. 6(b), a comparative high heat load of 140 W is applied. In comparison with the two figures, different heater surface temperature profiles are observed. Owing to a successful startup with heat load of 140 W in Fig. 6(b), the earlier accumulated liquid in the vapor channels vanishes. Thereafter, with the increase process, no decline of the heater surface temperature is observed.

Fig. 7 shows the data obtained from Fig. 6(a). It is very clear to find out that, with the initial distribution of working fluid being eliminated, a lower heater surface temperature is detected between 120 W and 60 W during the decreasing process.

In Fig. 8, different sequences of heat loads are designed and different pumping powers are selected. In the test run as presented in Fig. 8(a), the heat load is changed with the power cycle of 80 W–0 W–90 W–0 W–110 W–0 W–140 W–0 W–90 W–0 W–170 W–0 W–110 W in sequential order. Similarly, in Fig. 8(b), the heat load is varied with the power cycle of 60 W–0 W–90 W–0 W–110 W–0 W–100 W–0 W–90 W–0 W–110 W. The interval time between these two sequential orders exceeds 12 h. Before each heat load turns on, the system goes back to cold state. At 140 W as seen in Fig. 8(a), similar trends of heater surface temperature variation are observed. Thereafter, the initial distribution of liquid in the vapor channels vanishes. Comparing with the same heat load of 90 W in Fig. 8(a), different heater surface temperatures with values of 61.1 °C and 56.5 °C respectively are noted. This validates the fact that a lower operation temperature appears after the vanishing of the initial status of liquid in the evaporator. We can also notice that the temperature differences are at 110 W in Fig. 8(a) and 90 W in Fig. 8(b), respectively. With the same heat load of 110 W in Fig. 8(b), the heater surface temperature eventually kept the same value of 65.5 °C, while the variation of temperature profiles differs from each other due to the impact of the initial liquid distribution in the evaporator.

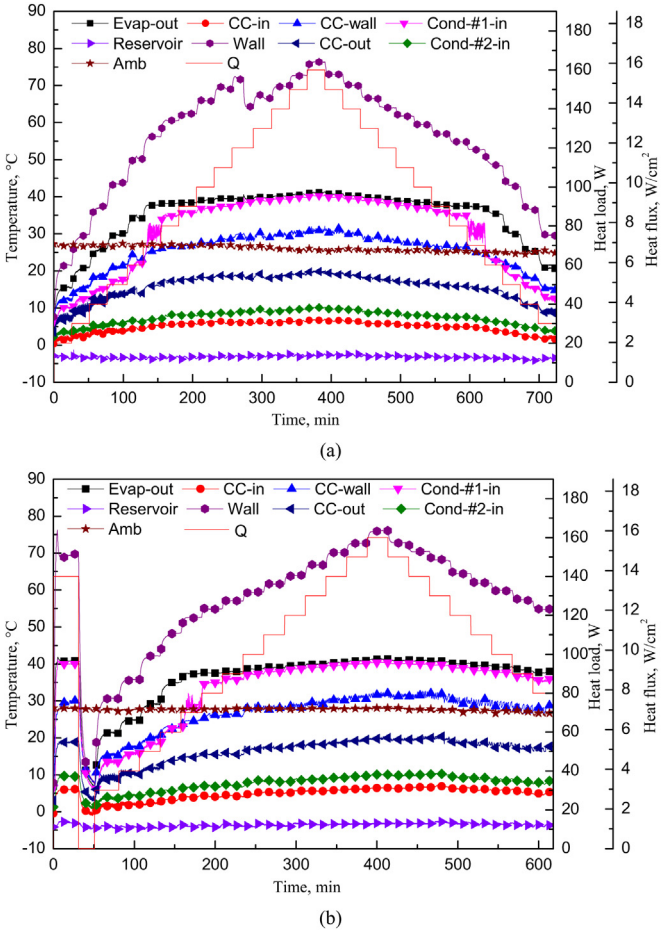

Fig. 6. Impact of initial distribution of working fluid in the evaporator with W_{pump} = 1.6 W, T_{sink} = −10 °C.

3.4. Operational characteristics of the system

In the present tests, different working conditions with various heat sink temperature and different pumping powers are carried out. The temperature indicated in Figs. 9 and 10 are recorded in steady state without the impact of initial status of liquid in the evaporator. Fig. 9 presents the evaporator outlet temperature against heat load at different heat sink temperature of −10 °C, 0 °C and 10 °C. From the slope of temperature curves, each curve in Fig. 9 can be divided into two segments, separately representing different phases of working fluid in the vapor chamber. A minor pumping power and a major heat sink temperature will lead to a premature turning point on the curve. At low heat loads, vapor chamber is filled with liquid. With the increase of the heat load, the evaporator

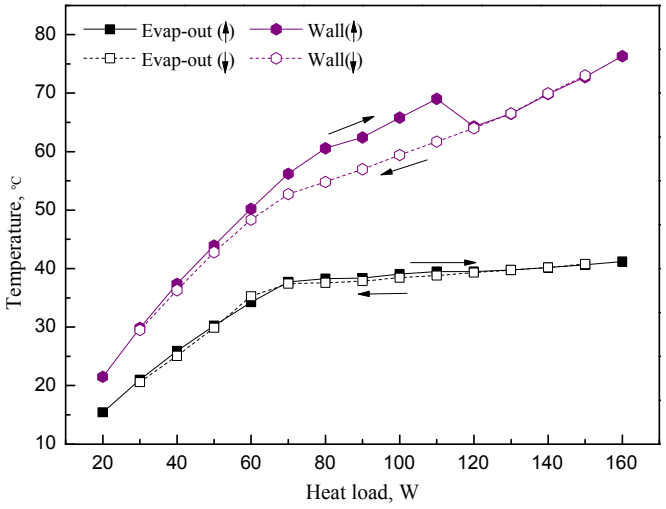

Fig. 7. Operation temperature with the heat load going up and down at W_{pump} = 1.6 W, T_{sink} = −10 °C.

outlet temperature of liquid increases rapidly. While under high heat loads, vapor displaces liquid in the vapor chamber, and then the evaporator outlet temperature of vapor increases within a narrow range. As seen at the same heat sink temperature, the vapor temperature remains approximately the same. It indicates that changing the pumping power has nearly no effect on the vapor temperature. Under the heat sink temperature of −10 °C, 0 °C and 10 °C, the vapor temperature is around 37.5 °C, 40 °C and 42.5 °C respectively. In other words, the vapor temperature declines gradually following the decrease of heat sink temperature.

Fig. 10 illustrates the variation of heater surface temperature against the heat load. The system reaches 180 W (heat flux = 17.7 W/cm^2) at the heater surface temperature below 80 °C. As presented clearly, a lower heater surface temperature is detected with the decreasing of the heat sink temperature, mainly because of a colder backflow of liquid into the compensation chamber. At the same heat sink temperature, the pumping power has a significant impact on the heater surface temperature under low heat loads. Under these circumstances, single-phase heat transfer is the prime heat transfer method. Therefore, increasing the liquid flow rate would enhance the efficiency of the heat transfer in the evaporator, resulting in a lower heater surface temperature. Under high heat loads, it seems that no obvious difference in the heater surface temperature at different pumping powers is observed. In this case, as mentioned earlier, two-phase heat transfer plays the dominant role, changing the pumping power doesn't affect the heater surface temperature significantly.

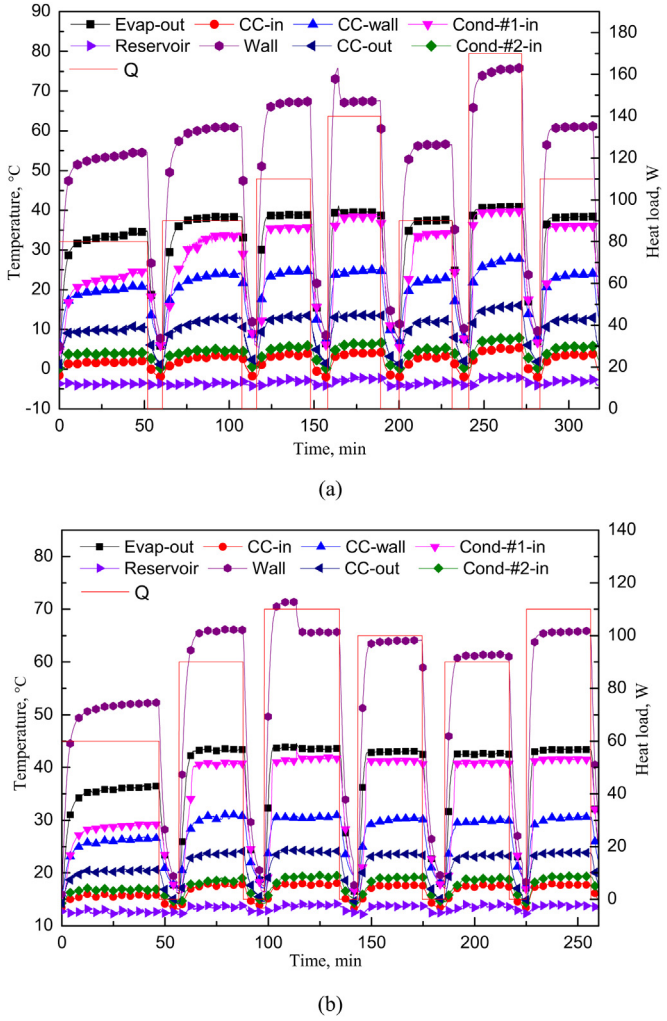

Fig. 8. Start-up tests of the system at different power cycles. (a) Sequential heat load cycle of 80 W–0 W–90 W–0 W–110 W–0 W–140 W–0 W–90 W–0 W–170 W–0 W–110 W, W_{pump} = 1.8 W, T_{sink} = −10 °C. (b) Sequential heat load cycle of 60 W–0 W–90 W–0 W–110 W–0 W–100 W–0 W–90 W–0 W–110 W, W_{pump} = 2 W, T_{sink} = 10 °C.

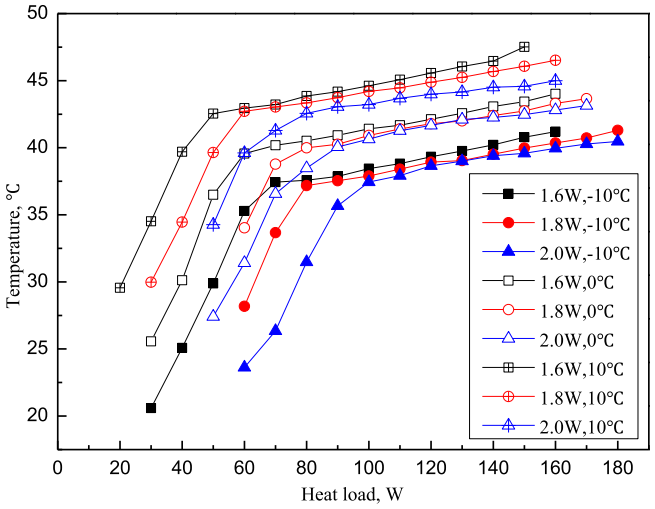

Fig. 9. The evaporator outlet temperature versus heat load at different pumping powers and heat sink temperature.

3.5. Thermal resistance

For evaluating the operational performance, the evaporator thermal resistance is defined as:

$$R_{evap} = \frac{T_{wall} - T_{evap-out}}{Q} \quad (1)$$

where, T_{wall} is the average temperature of the heater surface, $T_{evap-out}$ is the evaporator outlet temperature, Q is the input heat power.

The evaporator thermal resistance with different pumping powers at the heat sink temperature of −10 °C is presented in Fig. 11. The variation of the thermal resistance against the heat load represents the heat transfer performance in the vapor chamber. It

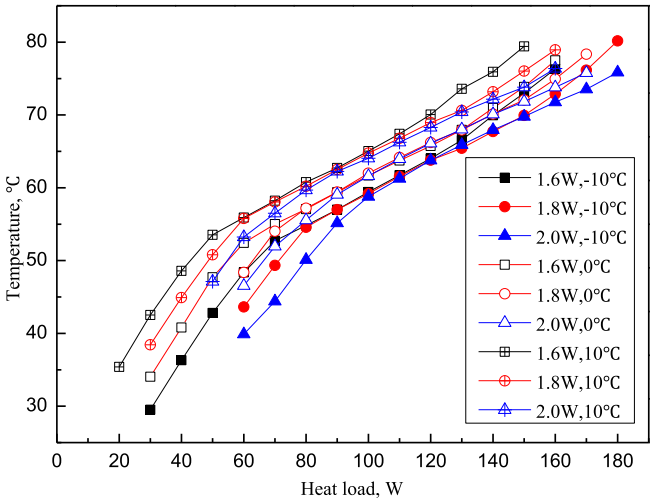

Fig. 10. Heater surface temperature versus heat load at different pumping powers and heat sink temperature.

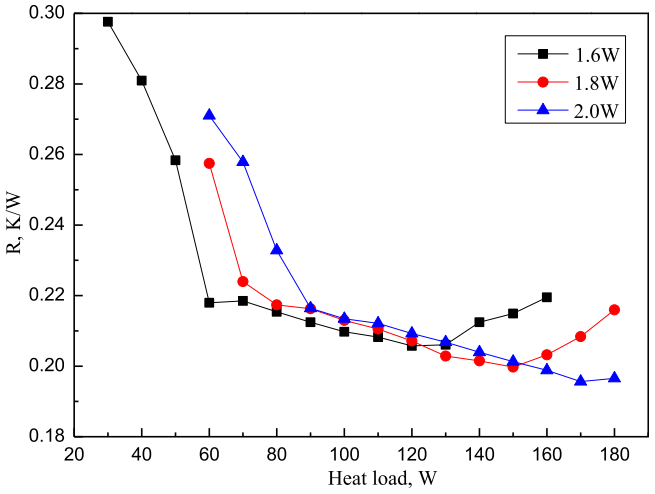

Fig. 11. The evaporator thermal resistance with different pumping powers at $T_{sink} = -10$ °C.

shows a typical trend of decreased evaporator thermal resistance following with increasing heat load. When the heat load reaches high enough, a slight increased thermal resistance is observed. For high heat loads, due to the superheating of vapor in the vapor chamber, the heat transfer performance gradually decreases. Thus, there is a slight increase of the thermal resistance. At the same heat load below 90 W, a lower thermal resistance is observed with the decreased pumping power. This is mainly caused by two factors: (1) As mentioned above, with the vapor chamber filled with liquid at low heat load, decreasing pumping power would weaken the efficiency of heat transfer in the compensation chamber, then a higher value of $T_{evap\text{-}out}$ is detected. Thus, a lower thermal resistance is calculated. (2) As the pumping power decreases, the menisci set up in the wick with a lower heat load. Hence, the phase change process takes a dominant role in the evaporator in advance and the thermal resistance sharply decreases. In Fig. 11, the evaporator thermal resistance varies between 0.298 K/W and 0.196 K/W.

4. Conclusions

In order to address the drawbacks of temperature oscillation and limited heat transport distance in LHP, this article proposed a pump-assisted capillary phase change loop equipped with a flat-disk-shaped evaporator. Accordingly, a particular investigation is carried out and the heat transfer performance was analyzed in detail. From extensive experimental tests, our conclusions can be summarized as follows:

1. The heat transport distance of the system reaches 1850 mm. The maximum heat load the system could transfer reaches 180 W (17.7 W/cm^2) when the heater surface temperature is below 80 °C.
2. Two different kinds of phase distribution in the vapor chamber appear under different working conditions. This can be deduced from the temperature difference between the evaporator outlet and the condenser #1 inlet.
3. The system shows a rapid response to the input power with no obvious temperature oscillation being observed.
4. The initial distribution of the working fluid in the evaporator has a great impact on the operation characteristics. A lower heater surface temperature will be detected during the operation process with a disappearance in the initial status.
5. A lower heat sink temperature corresponds to a minor evaporation temperature of the working fluid. When the phase change process takes place in the evaporator, the variation of the pumping power has little impact on the operation temperature.
6. At the heat sink temperature of −10 °C, the evaporator thermal resistance varies between 0.298 K/W and 0.196 K/W.

Acknowledgements

The current research was supported by the National Natural Science Foundation of China (Grant No. 51276071).

References

[1] Y.F. Maydanik, M.A. Chernysheva, V.G. Pastukhov, Review: loop heat pipes with flat evaporators, Appl. Therm. Eng. 67 (2014) 294–307.
[2] Y.F. Maydanik, Loop heat pipes, Appl. Therm. Eng. 25 (2005) 635–657.
[3] D. Gai, Z. Liu, W. Liu, J. Yang, Operational characteristics of miniature loop heat pipe with flat evaporator, Heat Mass Transfer 46 (2009) 267–275.
[4] T. Kaya, J. Ku, Thermal operational characteristics of a small-loop heat pipe, J. Thermophys. Heat Transfer 17 (2003) 464–470.
[5] V.G. Pastukhov, Y.F. Maidanik, C.V. Vershinin, M.A. Korukov, Miniature loop heat pipes for electronics cooling, Appl. Therm. Eng. 23 (2003) 1125–1135.
[6] R. Singh, A. Akbarzadeh, M. Mochizuki, Operational characteristics of the miniature loop heat pipe with non-condensable gases, Int. J. Heat Mass Transfer 53 (2010) 3471–3482.
[7] B.B. Chen, Z.C. Liu, W. Liu, J.G. Yang, H. Li, D.D. Wang, Operational characteristics of two biporous wicks used in loop heat pipe with flat evaporator, Int. J. Heat Mass Transfer 55 (2012) 2204–2207.
[8] Z. Liu, D. Gai, H. Li, W. Liu, J. Yang, M. Liu, Investigation of impact of different working fluids on the operational characteristics of miniature LHP with flat evaporator, Appl. Therm. Eng. 31 (2011) 3387–3392.
[9] J. Li, D. Wang, G.P. Peterson, Experimental studies on a high performance compact loop heat pipe with a square flat evaporator, Appl. Therm. Eng. 30 (2010) 741–752.
[10] Z. Liu, H. Li, B. Chen, J. Yang, W. Liu, Operational characteristics of flat type loop heat pipe with biporous wick, Int. J. Therm. Sci. 58 (2012) 180–185.
[11] H. Li, Z. Liu, B. Chen, W. Liu, C. Li, J. Yang, Development of biporous wicks for flat-plate loop heat pipe, Exp. Therm. Fluid Sci. 37 (2012) 91–97.
[12] J. Ku, L. Ottenstein, P. Rogers, K. Cheung, Investigation of Low Power Operation in a Loop Heat Pipe, 2001. SAE Paper No. 2001-01-2192.
[13] D. Mo, G. Zou, S. Lu, L. Zhang, A flow visualization study on the temperature oscillations inside a loop heat pipe with flat evaporator, in: ASME 2013 International Technical Conference and Exhibition on Packaging and Integration of Electronic and Photonic Microsystems, American Society of Mechanical Engineers, 2013.
[14] Y. Chen, M. Groll, R. Mertz, Y.F. Maydanik, S.V. Vershinin, Steady-state and transient performance of a miniature loop heat pipe, Int. J. Therm. Sci. 45 (2006) 1084–1090.
[15] J. Ku, Temperature oscillations in loop heat pipe operation, AIP Conf. Proc. 552 (2001) 255–262.
[16] R. Singh, A. Akbarzadeh, M. Mochizuki, Operational characteristics of a miniature loop heat pipe with flat evaporator, Int. J. Therm. Sci. 47 (2008) 1504–1515.
[17] X. Zhang, J. Huo, S. Wang, Experimental investigation on temperature oscillation in a miniature loop heat pipe with flat evaporator, Exp. Therm. Fluid Sci. 37 (2012) 29–36.
[18] D. Gai, W. Liu, Z. Liu, J. Yang, Temperature oscillation of mLHP with flat evaporator, Heat Transfer Res. 40 (2009) 321–332.
[19] N. Schweizer, P. Stephan, R. Schlitt, A Concept for a Miniature, Mechanically Pumped Two-phase Cooling Loop, 2008. SAE Paper No. 2008-01-1953.
[20] M. Crepinsek, C. Park, Experimental analysis of pump-assisted and capillary-driven dual-evaporators two-phase cooling loop, Appl. Therm. Eng. 38 (2012) 133–142.
[21] Y. Miyazaki, S. Oshima, M. Furukawa, R. Imai, Pump assisted heat pipe system, in: AIAA Thermophysics Plasmadynamics and Lasers Conference, 1988, San Antonio, Texas.
[22] T. Hoang, R. Baldauff, K. Cheung, Evaluation of a magnetically-driven bearingless pump for spacecraft thermal management, in: International Energy Conversion Engineering Conference, 2007. St Louis, Missouri.
[23] T. Hoang, R. Baldayff, K. Cheung, Hybrid Two-phase Mechanical Capillary Pumped Loop for High-capacity Heat Transport, 2007. SAE Paper No. 2007-01-3198.
[24] C. Park, M. Crepinsek, Effect of operational conditions on cooling performance of pump-assisted and capillary-driven two-phase loop, J. Thermophys. Heat Transfer 25 (2011) 572–580.
[25] C. Park, A. Vallury, J. Zuo, Performance evaluation of a pump-assisted, capillary two-phase cooling loop, J. Therm. Sci. Eng. Appl. 1 (2009) 022004.
[26] B.B. Chen, W. Liu, Z.C. Liu, H. Li, J.G. Yang, Experimental investigation of loop heat pipe with flat evaporator using biporous wick, Appl. Therm. Eng. 42 (2012) 34–40.
[27] www.njomp.cn.
[28] R.R. Riehl, T.C.P.A. Siqueira, Heat transport capability and compensation chamber influence in loop heat pipes performance, Appl. Therm. Eng. 26 (2006) 1158–1168.